

On-chip optimal Stokes nanopolarimetry based on spin-orbit interaction of light

Alba Espinosa-Soria¹, Francisco J. Rodríguez-Fortuño², Amadeu Griol¹ and Alejandro Martínez^{1*}

¹Nanophotonics Technology Center, Universitat Politècnica de València, Valencia, Spain

²Department of Physics, King's College London, Strand, London WC2R 2LS, United Kingdom

* email: amartinez@ntc.upv.es

Supporting Information

S.1. Transverse spin in multimode silicon waveguides

To demonstrate the performance of the proposed Stokes nanopolarimeter we have used silicon waveguides with rectangular cross-section (220 nm thickness and different widths), being the silicon core completely surrounded by silica. Such waveguides can be fabricated using mainstream semiconductor fabrication tools and processes (see section S.4). For a silicon core width of 360 nm (as in the case of the optimal nanopolarimeter) only two guided modes propagate in the wavelength region around $\lambda=1550\text{nm}$, as depicted in Fig. S1. Such modes are typically used in integrated silicon photonics circuitry: the fundamental even or TE-like mode (characterized by a main electric field component along y), and the fundamental odd or TM-like mode (characterized by a main electric field component along z).

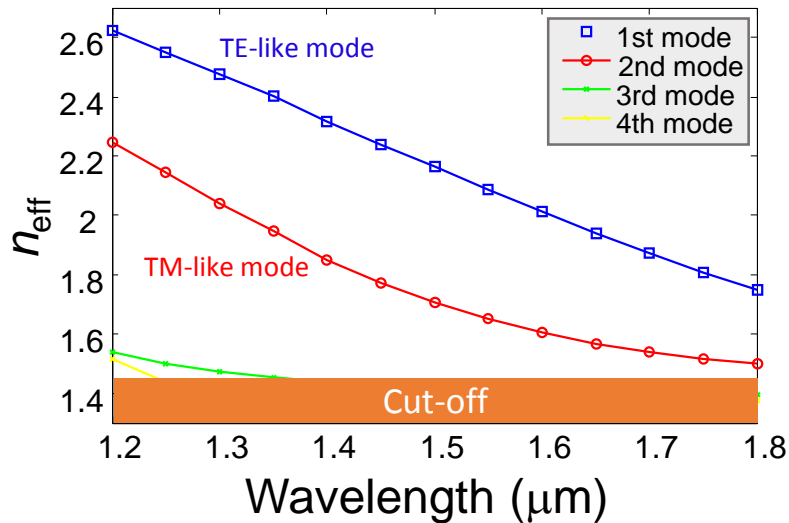


Figure S1. Effective index (n_{eff}) of the guided modes of a silicon waveguide with 220x360 nm cross section surrounded by silica in the wavelength region between 1.2 and 1.8 μm . Calculations have been performed using a finite-element method implemented in the commercial package FemSIMTM by RSoft. A grid size of 20 nm has been considered.

The cross-sections of the three electric field components for the two fundamental guided modes considering propagation along positive values of the x -axis (forward or + propagation) are shown in Fig. S2 at $\lambda=1550\text{ nm}$. We have checked that the different field components display a similar

distribution – remarkably, the symmetries with respect to the main axes remain identical - for other core dimensions as well as at other wavelengths. Moreover, such field profiles are also retained for an asymmetric configuration in which the waveguide core is not up-covered with silica. A remarkable longitudinal field component responsible for transverse spin as well as SOI-related phenomena is observed in all the cases, both outside (evanescent field) and inside the waveguide silicon core [1]. Notice that this component of the electric field (E_x) will reverse its sign for backward propagation (towards $-x$), which is a clear signature of the spin-momentum locking or QSHE of light intrinsic to both evanescent and guided waves [2]. The cross-sectional maps are distinct for different modes, which ensures encoding of the incident polarization into different optical intensities coupled towards backward and forward directions for each considered mode. This enables the realization of distinct measurements on the SoP, as required in polarimeters. Additional guided modes propagate at lower wavelengths as shown in Fig. S1. Increasing the size of the waveguide core cross-section would allow the appearance of more guided modes at the wavelength region around 1550 nm. All such guided modes would also show transverse spin but different field profiles, being useful to perform additional polarimetric measurements. For the simplest case of a single straight waveguide with a coupled scatterer, if the waveguide supports M guided modes (with $M \geq 2$), the resulting matrix \mathbf{W} would have dimensions $2M \times 4$, being $2M \geq 4$. Of course, the number of measurements for a single SoP (and therefore in a single shot) could be further increased by using more waveguides, which leads us to the general polarimeter scheme shown in Fig. 1a. In general, increasing the number of measurements –via either extra modes or additional waveguides - per input SoP is useful to reduce noise-induced errors in the retrieval of the Stokes parameters [3][4].

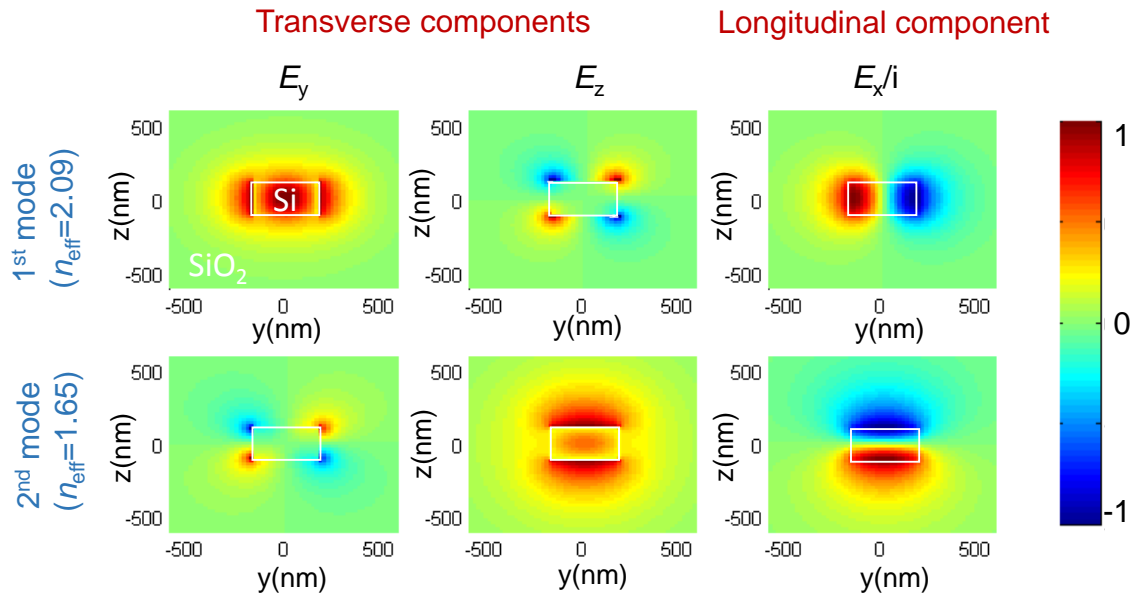


Figure S2. Numerically calculated cross-sectional profiles of the electric field components of the first two propagating modes in a silicon waveguide (360 nm x 220 nm cross-section) surrounded by silica at $\lambda = 1550$ nm. Left panels: E_y component; Middle panels: E_z component; Right panels: E_x divided by the imaginary unit (longitudinal field responsible for transverse spin and SOI related effects). The solid white rectangle highlights the boundary between the silicon core and the surrounding silica cladding.

S.2. Theory and performance of the Stokes nanopolarimeter based on SOI

a) Polarization-dependent effective area of a scatterer with several output ports and modes

As shown in Fig. 1a, the scatterer-waveguide system performing as a Stokes nanopolarimeter is normally illuminated by a monochromatic transverse light beam whose electric field may be generally written as [5]:

$$\mathcal{E}^{inc}(\vec{r}) = (E_x^{inc}(x, y)\hat{x} + E_y^{inc}(x, y)\hat{y})\exp(-ikz) = A \frac{(\hat{x}+m\hat{y})}{\sqrt{1+|m|^2}} \exp(-ik_0z) \quad (2.1)$$

where $A(x, y)$ is the wave amplitude at every point, k_0 is the wave number and the complex number $m(x, y)$ determines the SoP (which, remarkably, may vary across the beam). Indeed, the parameter m is related to all the ideal polarizations used to define the Stokes parameters. In our coordinate system, $m = 0$ in horizontal linear polarization (I_H), $m = \infty$ in vertical linear polarization (I_V), $m = 1$ in 45° linear polarization (I_{45}), $m = -1$ in 135° linear polarization (I_{135}), $m = i$ in left-handed circular polarization (I_L), and $m = -i$ in right-handed circular polarization (I_R). Notice that we are assuming that the input wave is purely transversal and it does not have longitudinal components of the electric field (this approximation is valid for non-tightly focused beams). The beam will impinge on our subwavelength scatterer (notice that the scatterer could be in principle as small as a single atom), so we can consider it *locally* as a plane wave with a certain power density $I^{inc} = |A|^2/2\eta$, where η is the medium impedance, and a fixed polarization identified through its normalized Jones vector as follows:

$$\hat{\mathbf{E}}^{inc} = \begin{pmatrix} \hat{E}_x^{inc} \\ \hat{E}_y^{inc} \end{pmatrix} = \frac{1}{\sqrt{1+|m|^2}} \begin{pmatrix} 1 \\ m \end{pmatrix}. \quad (2.2)$$

In the general case, the incident wave defined by Eq. (2.2) impinges on a very small scatterer coupled to several waveguides or ports, where each waveguide may support a variable number of electromagnetic modes (see Fig. 1a). Notice that, in our scheme, a single straight waveguide in the proximity of the scatterer has two propagation directions, and therefore, two associated ports. It is in principle possible to measure individually the optical power excited in each port-mode combination, which we call P_k for the k -th port-mode combination. P_k will be proportional to the incident power density I_{inc} on the scatterer, with a proportionality constant termed the *effective area*, so our scatterer can be considered to operate as an optical antenna. Thanks to SOI, the effective area for the k -th port-mode combination will depend on the incident polarization such that:

$$P_k = I_{inc} A_{eff}^k(m). \quad (2.3)$$

The SOI-related dependence of the effective area on the SoP can be completely described by studying the amplitude and phase of the mode excitation under incidence of two orthogonal polarizations. For simplicity we will assume horizontal H (along x) and vertical V (along y) linear polarizations. For H incidence, the amplitude and phase of the mode that is excited at the k -th port-mode combination can be characterized by a complex number l_H^k , such that the power excited is $P_k = I_{inc} |l_H^k|^2$. Similarly we get $P_k = I_{inc} |l_V^k|^2$ for V incidence. We term l_H^k and l_V^k the *complex effective lengths* for the k -th port-mode combination, being these complex amplitudes closely related to the scattering-parameter matrix commonly used in engineering. In general, any incident

polarization is a linear superposition of the two orthogonal states, so the excited power can be obtained by linear superposition (taking into account the phase) as:

$$P_k = I_{\text{inc}} |\hat{\mathbf{E}}_x^{\text{inc}} l_H^k + \hat{\mathbf{E}}_y^{\text{inc}} l_V^k|^2. \quad (2.4)$$

Comparing (2.3) with (2.4) allows us to write the effective area as the square of a dot product between a normalized Jones vector and a vector with the complex effective lengths:

$$A_{\text{eff}}^k(m) = \left| \begin{pmatrix} \hat{\mathbf{E}}_x^{\text{inc}} \\ \hat{\mathbf{E}}_y^{\text{inc}} \end{pmatrix} \cdot \begin{pmatrix} l_H^k \\ l_V^k \end{pmatrix} \right|^2 \equiv |\hat{\mathbf{E}}^{\text{inc}} \cdot \mathbf{l}^k|^2 \quad (2.5)$$

A dot product is maximum whenever the two vectors are complex conjugates of one another. This motivates us to introduce definitions that allow us to re-write (2.3) and (2.5) into an intuitive form:

$$\left\{ \begin{array}{l} P_k = I_{\text{inc}} A_{\text{max}}^k \overbrace{|\hat{\mathbf{E}}^{\text{inc}} \cdot (\hat{\mathbf{E}}_{\text{max}}^k)^*|^2}^{\in [0,1]} \\ A_{\text{max}}^k \equiv |\mathbf{l}^k|^2 \\ \hat{\mathbf{E}}_{\text{max}}^k \equiv \frac{1}{|\mathbf{l}^k|} (\mathbf{l}^k)^* \end{array} \right., \quad (2.6)$$

where $\hat{\mathbf{E}}_{\text{max}}^k$ corresponds to the incident polarization that maximizes the power output on the k -th mode: $\max(P_k) = I_{\text{inc}} A_{\text{max}}^k$.

It is crucial to realize that, thanks to SOI, *the polarization $\hat{\mathbf{E}}_{\text{max}}^k$ can be different for each port-mode combination* (this requires breaking the mirror symmetry in our system, as discussed below), so that each k -th power measurement will be proportional to the geometric projection of the incident polarization Jones vector to the polarization vector $\hat{\mathbf{E}}_{\text{max}}^k$.

b) Variation of effective areas across the Poincaré sphere

We now consider how the power P_k varies across the Poincaré sphere of incident polarizations. In general, the Stokes vector $\mathbf{S}(\mathbf{E})$ associated to any polarization Jones vector \mathbf{E} is given by:

$$\mathbf{S}(\mathbf{E}) = \begin{pmatrix} S_0 \\ S_1 \\ S_2 \\ S_3 \end{pmatrix} = \begin{pmatrix} I_H + I_V \\ I_H - I_V \\ I_{45} - I_{135} \\ I_L - I_R \end{pmatrix} = \begin{pmatrix} |E_x|^2 + |E_y|^2 \\ |E_x|^2 - |E_y|^2 \\ 2 \operatorname{Re}(E_x E_y^*) \\ -2 \operatorname{Im}(E_x E_y^*) \end{pmatrix}. \quad (2.7)$$

Any fully polarized field can be mapped into the surface of the Poincaré unit sphere with the coordinates of the normalized 3D Stokes vector:

$$\hat{\mathbf{s}}(\mathbf{E}) = \frac{1}{s_0} \begin{pmatrix} S_1 \\ S_2 \\ S_3 \end{pmatrix} \quad (2.8)$$

Starting from these definitions, with some algebra it can be verified that there is a mathematical relation between the squared dot product of any two Jones vectors and the dot product of the corresponding Stokes vectors:

$$|\mathbf{E}_a \cdot (\mathbf{E}_b)^*|^2 = \frac{1}{2} [\mathbf{S}(\mathbf{E}_a) \cdot \mathbf{S}(\mathbf{E}_b)], \quad (2.9)$$

and with further algebra (realizing that when light is totally polarized $|\mathbf{E}|^2 = S_0^2 = S_1^2 + S_2^2 + S_3^2$), we can obtain a corresponding relation between the dot product of the Jones vectors and the angle θ subtended at the origin of the Poincaré sphere by the two vectors $\hat{\mathbf{S}}(\mathbf{E}_i)$:

$$\begin{aligned} |\mathbf{E}_a \cdot (\mathbf{E}_b)^*|^2 &= |\mathbf{E}_a|^2 |\mathbf{E}_b|^2 \left[\frac{1}{2} (\hat{\mathbf{S}}(\mathbf{E}_a) \cdot \hat{\mathbf{S}}(\mathbf{E}_b) + 1) \right] \\ &= |\mathbf{E}_a|^2 |\mathbf{E}_b|^2 \cos^2(\theta/2), \end{aligned} \quad (2.10)$$

Equations (2.9) and (2.10) are general mathematical identities relating arbitrary polarizations and their Stokes vectors. Using them, we can re-write the power at the k -th port-mode combination in terms of the Stokes vectors and in terms of the angle between polarizations in the Poincaré sphere:

$$\begin{aligned} P_k &= I_{\text{inc}} A_{\text{max}}^k |\hat{\mathbf{E}}^{\text{inc}} \cdot (\hat{\mathbf{E}}_{\text{max}}^k)^*|^2 \\ &= I_{\text{inc}} A_{\text{max}}^k \frac{1}{2} [\mathbf{S}(\hat{\mathbf{E}}_{\text{max}}^k) \cdot \mathbf{S}(\hat{\mathbf{E}}^{\text{inc}})], \\ &= I_{\text{inc}} \underbrace{A_{\text{max}}^k \cos^2(\theta_k/2)}_{A_{\text{eff}}^k(m)} \end{aligned} \quad (2.11)$$

where $\theta_k(\hat{\mathbf{E}}^{\text{inc}})$ is the angle subtended at the origin of the Poincaré sphere between the polarizations $\hat{\mathbf{E}}^{\text{inc}}$ and $\hat{\mathbf{E}}_{\text{max}}^k$. From Eq. (2.11) we can easily calculate the effective area of the k -th port-mode combination on the whole surface of the Poincaré sphere, corresponding to every possible SoP of the incident beam. This is shown in Fig. S3. In principle, every port-mode combination is associated with a plot similar to Fig. S3 at each wavelength, which depends only on the port, mode and wavelength-dependent $\hat{\mathbf{E}}_{\text{max}}^k$. Notice that the effective area is maximum for the polarization $\hat{\mathbf{E}}_{\text{max}}^k$ defined in (2.6), and it is exactly zero for the polarization that lies in the antipodal point in the Poincaré sphere, which corresponds to $\hat{\mathbf{E}}_0^k = |\mathbf{l}_k|^{-1}(-l_V^k, l_H^k)^T$, such that $A_{\text{eff}}^k(\hat{\mathbf{E}}_0^k) = 0$.

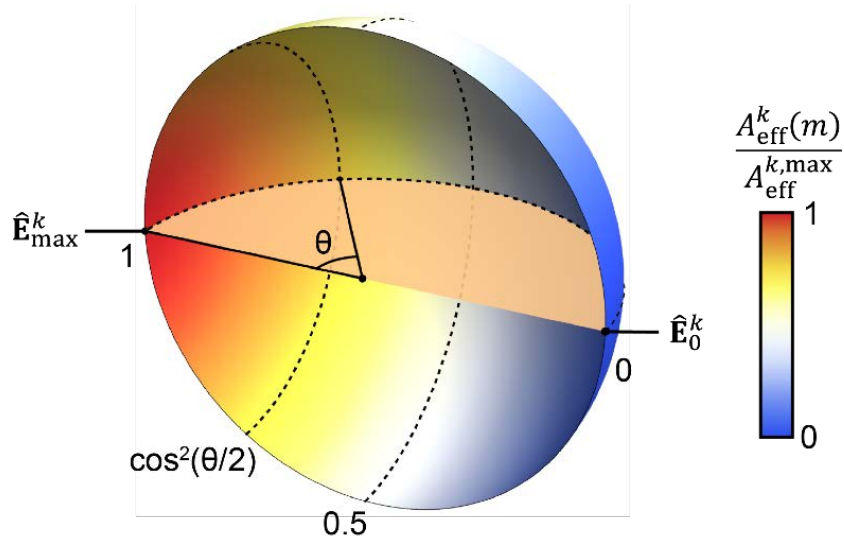


Figure S3. Plot of the normalised polarization-dependent effective area as a function of the incident polarization, represented in a cross-section of the Poincaré sphere of incident polarizations.

c) Matrix polarimeter equation in terms of effective areas

Equation (2.11) is crucial in our polarimetric approach since it tells us that the power output of the k -th port-mode combination is a linear combination of the Stokes parameters of incident light polarization. Thus it constitutes the k -th row in a matrix that relates the S-parameters of the incident field (vector $\mathbf{S}(\hat{\mathbf{E}}_{\text{inc}})$ of length 4) to the power measured for the outputs $k = 1 \dots N$ (vector \mathbf{P} of length N):

$$\mathbf{P} = I_{\text{inc}} \mathbf{W} \mathbf{S}(\hat{\mathbf{E}}_{\text{inc}}), \quad (2.12)$$

where, from (2.11), the k -th row in the polarimetric (or instrument) matrix \mathbf{W} is given by:

$$\mathbf{a}_k = \frac{1}{2} A_{\text{max}}^k \mathbf{S}(\hat{\mathbf{E}}_{\text{max}}^k)^T. \quad (2.13)$$

Notice that, from the definitions in (2.6) and (2.7) we can re-write this vector as $\mathbf{a}_k = \frac{1}{2} \mathbf{S}(\mathbf{I}^{k*})^T$, which applying the definition of Stokes parameters from (2.7) yields:

$$\mathbf{a}_k = \frac{1}{2} (|l_H^k|^2 + |l_V^k|^2 \quad |l_H^k|^2 - |l_V^k|^2 \quad |l_{45}^k|^2 - |l_{135}^k|^2 \quad |l_R^k|^2 - |l_L^k|^2), \quad (2.14)$$

where we defined $l_{45}^k = (l_H^k + l_V^k)/\sqrt{2}$, $l_{135}^k = (l_H^k - l_V^k)/\sqrt{2}$, $l_R^k = (l_H^k - il_V^k)/\sqrt{2}$ and $l_L^k = (l_H^k + il_V^k)/\sqrt{2}$, which correspond to the complex amplitude of the mode excited under illumination of the corresponding polarizations. Notice that the sign of S_3 was reversed due to the complex conjugation of \mathbf{I}^k . From (2.4) this can be re-written in terms of the effective areas of the scatterer for the pure polarizations associated with the different m parameters:

$$\mathbf{a}_k = \frac{1}{2} (A_{\text{eff}}^k(0) + A_{\text{eff}}^k(\infty) \quad A_{\text{eff}}^k(0) - A_{\text{eff}}^k(\infty) \quad A_{\text{eff}}^k(1) - A_{\text{eff}}^k(-1) \quad A_{\text{eff}}^k(-i) - A_{\text{eff}}^k(i)). \quad (2.15)$$

In order to use the polarimeter to calculate the incident Stokes vector from the measured powers, i.e. inverting the matrix equation (2.12), we need a non-singular matrix \mathbf{W} , with at least four linearly independent rows [6].

d) Importance of symmetry breaking in the scatterer-waveguide system

Breaking of symmetry is fundamental for SOI effects to allow the splitting of elliptical polarizations into different waveguide port-mode combinations. If the scatterer-waveguides system is mirror symmetric with respect to a plane that contains the incidence direction, and this plane also contains the propagation direction of one of the output ports, then it follows that the two circular polarizations must excite that port equally, because the mirror symmetry exchanges left-handed and right-handed incident polarizations while leaving the structure unchanged. Therefore, $A_{\text{eff}}^k(-i) = A_{\text{eff}}^k(i)$ which implies $S_3(\hat{\mathbf{E}}_{\text{max}}^k) = 0$, so that the polarization $\hat{\mathbf{E}}_{\text{max}}^k$ must be linear. In fact, simple symmetry considerations show that this linear polarization will be either parallel or perpendicular to the plane of symmetry containing the port, depending on the port mode symmetry. If two ports are contained in the same mirror symmetry plane, they will both share the same linear polarization $\hat{\mathbf{E}}_{\text{max}}^k$ for the same modes (except for at most a time phase difference), and thus will not result in independent rows in the polarimetric matrix.

In the simplest case studied in this work (a straight waveguide with two ports with two guided modes each) we have to break mirror symmetry with respect to the plane containing each port

propagation direction, in order to split four different input polarizations into each port-mode combination. For this reason the structure in Fig. S4a would not work as polarimeter, but that in Fig. S4b would. From the point of view of SOI, it could be stated that the effects produced by each scatterer (each one placed in a region having longitudinal field component of opposite signs) in the symmetric configuration would cancel each other, thus avoiding spin-controlled directional guiding phenomena. This finding is verified by calculating the effective areas resulting from different input polarizations for both structures, as shown in Fig. S5. It can be seen that when the scatterer-waveguide system displays mirror symmetry the effective areas for the polarization pairs $(m = 1, m = -1)$ and $(m = i, m = -i)$ are identical for each mode, which would result in a non-invertible matrix \mathbf{W} after applying (2.15).

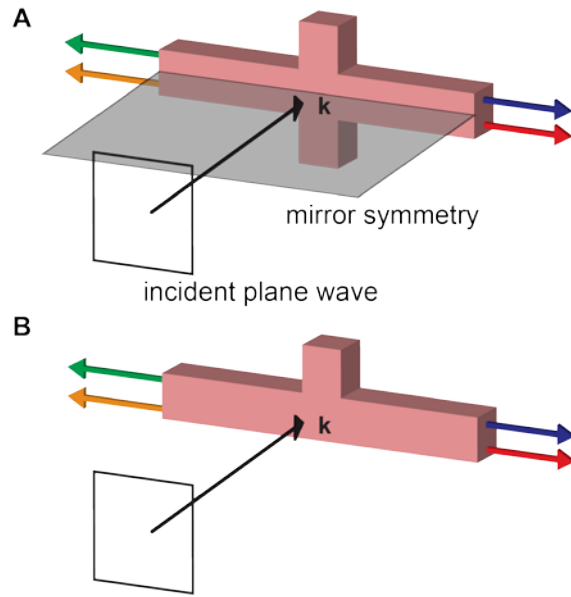


Figure S4. (a) Structure with mirror-symmetry on a plane containing the ports will not work as a polarimeter. All outputs in the ports will have a linearly polarized $\hat{\mathbf{E}}_{\max}^k$. (b) Breaking the mirror symmetry allows the split of non-parallel polarizations into the four port-mode combinations, enabling its use as a Stokes polarimeter.

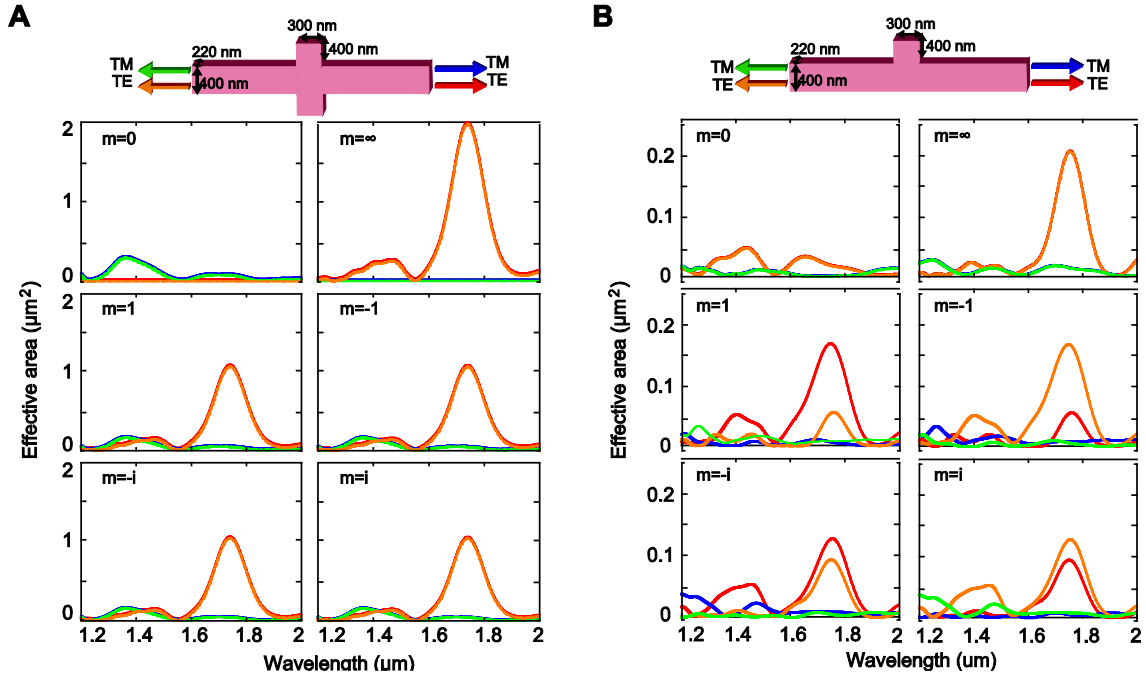


Figure S5. Effective areas of the four port-mode combinations for different input polarizations ($m=0, \infty, 1, -1, i, -i$) as a function of the wavelength. When the structure has mirror symmetry (a) the effective areas are equal in both outputs ports for each waveguide mode in all input polarization cases and all wavelengths. This can be attributed to the cancellation of the SOI effects. The situation changes when the mirror symmetry is broken (b), so that SOI produces that the obtained effective areas are different for each output-mode combination. Numerical simulations have been performed using CST Microwave Studio.

d) Theoretical requirements of the optimal polarimeter

In order for the structure to work as a Stokes polarimeter, Eq. (2.12) needs to be inverted to retrieve the Stokes vector given the vector of measurements. This requires matrix \mathbf{W} to be invertible, as mentioned above. In the simplest structure considered in this work (Fig. 1b), we have a straight silicon waveguide with two ports (x_+ and x_-) supporting two guided modes each (TE and TM), so all four rows, corresponding to the Stokes vector of \mathbf{I}^{k*} for the two directions and two modes, need to be independent. This means that the four polarizations $\hat{\mathbf{E}}_{max}^k$ must be different, which can be achieved by breaking the mirror symmetry, as shown in Figs. S4-S5. Therefore, any kind of asymmetry with respect to the xz plane will be sufficient to give an invertible matrix \mathbf{W} . This means that there is an infinite number of possible scatterer-waveguide systems that work as a polarimeter, so in this sense, our system is extremely robust against fabrication inaccuracies or disorder. However, the performance of all these polarimeters will be different. It is intuitive to see that, for the measurement to be as robust as possible with respect to noise in the measurement, firstly the effective areas need to be as big as possible, and secondly the different polarizations $\hat{\mathbf{E}}_{max}^k$ need to be as different as possible. Mathematically this second criterion is formally expressed by requiring the matrix \mathbf{W}^{-1} to have the smallest possible condition number κ , defined by:

$$\kappa(\mathbf{W}) = \|\mathbf{W}^{-1}\|_2 \|\mathbf{W}\|_2 \quad (2.16)$$

where $\|\cdot\|_2$ stands for the Euclidean norm. For the polarimetric matrix of a generic polarimeter, the minimum condition number is $(M - 1)^{1/2}$, where M corresponds to the Stokes vector dimension [7]. In the special case that the four maximum effective areas for the four outputs A_{\max}^k are equal, the minimization of $\kappa(\mathbf{W})$ depends exclusively on the polarizations sorted by each output $\hat{\mathbf{E}}_{\max}^k$. For these polarizations to be as different as possible, and thus achieve a minimum condition number, it was shown that the volume occupied by the tetrahedron whose vertices are the four $\hat{\mathbf{s}}(\hat{\mathbf{E}}_{\max}^k)$ on the Poincaré sphere has to be maximum [7][8]. This is achieved when the inscribed tetrahedron is a regular tetrahedron.

In order to find the optimal SOI polarimeter, we need to design the four $\hat{\mathbf{E}}_{\max}^k$ to be the vertices of a regular tetrahedron in the Poincaré sphere while having the same effective area A_{\max}^k . For simplicity, we decided to keep our structure $x = 0$ mirror symmetric, which means that the polarizations $\hat{\mathbf{E}}_{\max}^k$ associated to opposite ports for a given mode (TM or TE) must follow that same mirror symmetry. An $x = 0$ mirror symmetry in polarizations is equivalent to changing the sign of Stokes parameters S_2 and S_3 while keeping the sign of S_1 . Notice that, in contrast, the metasurface polarimeter in [9] only reverses the sign of S_3 , which impedes the formation of a tetrahedron with non-zero volume inside the Poincaré sphere. This introduces a restriction in our design, by making the pair of polarizations associated with TE waveguide modes $\hat{\mathbf{E}}_{\max}^{TE,x+}$, $\hat{\mathbf{E}}_{\max}^{TE,x-}$ propagating in opposite directions to be necessarily mirror symmetric of each other and thus show 180° rotation symmetry around axis S_1 in the Poincaré sphere. The two TM waveguide outputs $\hat{\mathbf{E}}_{\max}^{TM,x+}$, $\hat{\mathbf{E}}_{\max}^{TM,x-}$ will also show an identical relation. Given this restriction, the optimal polarizations must generate a regular tetrahedron in the Poincaré sphere that itself fulfills the same 180° rotation symmetry around axis S_1 . The solutions that fulfil this condition for optimality are given by:

$$\begin{aligned} \hat{\mathbf{s}}(\hat{\mathbf{E}}_{\max}^1) &= \frac{1}{5} \begin{pmatrix} 3 \\ 4 \cos(\alpha) \\ 4 \sin(\alpha) \end{pmatrix} \leftrightarrow \hat{\mathbf{s}}(\hat{\mathbf{E}}_{\max}^2) = \frac{1}{5} \begin{pmatrix} 3 \\ -4 \cos(\alpha) \\ -4 \sin(\alpha) \end{pmatrix}, \\ \hat{\mathbf{s}}(\hat{\mathbf{E}}_{\max}^3) &= \frac{1}{5} \begin{pmatrix} 3 \\ 4 \cos(\alpha + \pi/2) \\ 4 \sin(\alpha + \pi/2) \end{pmatrix} \leftrightarrow \hat{\mathbf{s}}(\hat{\mathbf{E}}_{\max}^4) = \frac{1}{5} \begin{pmatrix} 3 \\ -4 \cos(\alpha + \pi/2) \\ -4 \sin(\alpha + \pi/2) \end{pmatrix} \end{aligned} \quad (2.16)$$

with the corresponding Jones' vectors:

$$\begin{aligned} \hat{\mathbf{E}}_{\max}^1 &= \frac{1}{\sqrt{5}} \begin{pmatrix} 2e^{-i\alpha} \\ 1 \end{pmatrix} \leftrightarrow \hat{\mathbf{E}}_{\max}^2 = \frac{1}{\sqrt{5}} \begin{pmatrix} -2e^{-i\alpha} \\ 1 \end{pmatrix} \\ \hat{\mathbf{E}}_{\max}^3 &= \frac{1}{\sqrt{5}} \begin{pmatrix} ie^{-i\alpha} \\ 2 \end{pmatrix} \leftrightarrow \hat{\mathbf{E}}_{\max}^4 = \frac{1}{\sqrt{5}} \begin{pmatrix} -ie^{-i\alpha} \\ 2 \end{pmatrix} \end{aligned} \quad (2.17)$$

where the free parameter α represents a rotation of the polarizations around the S_1 axis in the Poincaré sphere. Figure S6 shows two particular examples of optimal polarizations with $\alpha = 0$ and $\alpha = \pi/4$ respectively. Notice that all four polarizations fulfill $S_1 = \pm 3/5$, with opposite signs associated to the different pairs. We are free to choose the sign for the S_1 parameter of the TE modes, and the opposite sign must then be designed for the TM modes. The tetrahedron can be rotated freely around the S_1 axis (parameter α) while keeping the required symmetry, but it is evident that rotation of the tetrahedron around any other axis would break that symmetry, graphically showing that this is the only solution. Supporting Movie 1 shows the collection of possible optimal polarizations and their associated tetrahedron in the Poincare sphere.

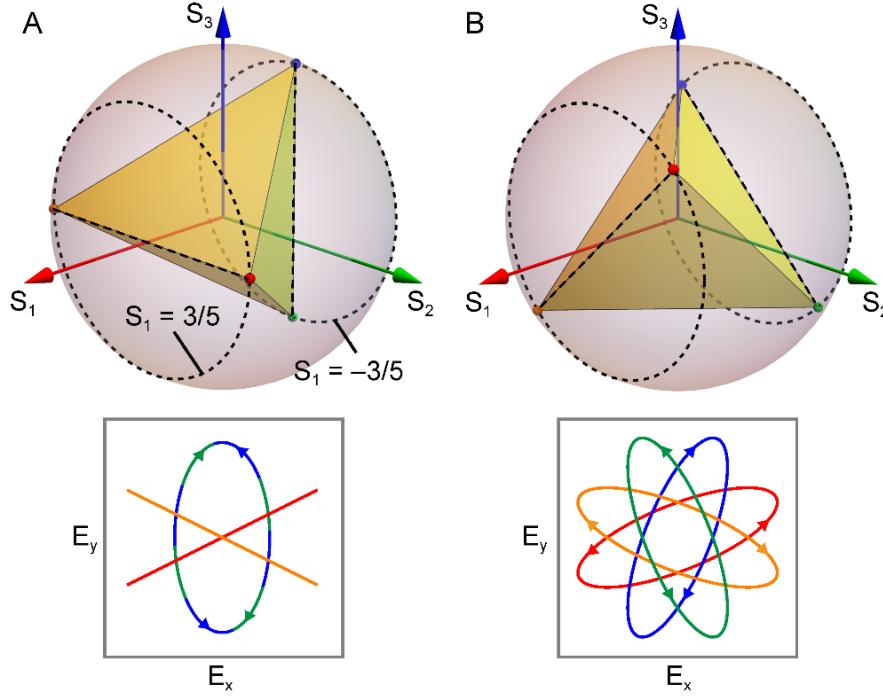


Figure S6. Optimal SOI nanopolarimeter. Optimal polarizations shown as polarization ellipses and as tetrahedrons in the Poincaré sphere following Eq. (2.16) for (a) $\alpha = 0$ and (b) $\alpha = \pi/4$.

S.3. Optimization of the Stokes nanopolarimeter

In the previous section, we have demonstrated that a SOI-based Stokes polarimeter can perform optimally. However, this requires a smart design of the scatterer-waveguide system in order to accomplish the criteria given by (2.16) and (2.17). In our quest for the optimal polarimeter, we started from the structure that we had previously used in Refs.[10],[11] – a rectangular protrusion in a silicon waveguide - because of its fabrication simplicity, the absence of metals (which can introduce absorption losses at the expenses of larger effective areas) and, remarkably, its capability to sort out linear-polarized waves at certain polarization angles for the TE modes, which in principle could satisfy (2.16). Since the basic structure (which we call rectangular-shape scatterer) is not optimal, we used the so-called simplex optimization method in MATLAB, together with full vectorial simulations performed with CST Microwave Studio. The Simplex method is an iterative algorithm for the minimization of a target function by varying a finite set of parameters. Starting from the value of the target function at a given point, the procedure consists of seeking for another point that improves the previous value. These points are vertexes of a N-dimensional polytope in the parameter space, that constitutes the region determined by the restrictions to which the problem is subject to (the so called feasible region). The search is performed by means of displacements of the edges of the polytope, from the current vertex up to the adjacent one, so that it improves the target value of the function. We decided to optimize the size and shape of the scatterer, converting the rectangular scatterer into a T-block shaped scatterer in order to have more variable parameters. Notice that, in principle, there are many other shapes that could end up in an optimal nanopolarimeter. As explained above, the SOI polarimeter is considered optimal when the four $\hat{\mathbf{E}}_{\max}^k$ describe a regular tetrahedron in the Poincaré sphere and the two maximum effective areas $\mathbf{A}_{\max}^{\text{TM}}$ and $\mathbf{A}_{\max}^{\text{TE}}$ are equal, so the target of the optimization was to maximize the volume of the tetrahedron (given by $\hat{\mathbf{E}}_{\max}^k$) while keeping equal effective areas.

In Fig. 2 we show the evolution of the optimizer along each iteration, starting from the studied rectangular shape scatterer and reaching an optimal T-block shaped scatterer design with a volume of 99.7% of a regular tetrahedron and a difference between effective areas of 2.7%.

S.4. Fabrication methods

The silicon nanopolarimeters were fabricated on standard silicon-on-insulator samples from SOITEC wafers with a top silicon layer thickness of 220 nm and a buried oxide layer thickness of 2 μm for the case of the single-waveguide polarimeters (either with rectangular or T-block scatterers). In the case of the cross-waveguide samples, we used a 250 nm silicon core on top of a 3 μm buried oxide substrate. Patterns were defined by using an electron-beam direct-writing process performed on a coated 100 nm hydrogen silsesquioxane (HSQ) resist film. The electron-beam exposure, performed with a Raith150 tool, was optimized to reach the required dimensions employing an acceleration voltage of 30 keV and an aperture size of 30 μm . After developing the HSQ film using tetramethylammonium hydroxide, the resist patterns were transferred into the samples by employing an optimized Inductively Coupled Plasma-Reactive Ion Etching process with fluoride gases. In the case of the cross-waveguide sample, we needed to add a metallic scatterer on top of the crossing. To this end, after silicon etching, a second e-beam exposure prior to a metal evaporation (40 nm of Au) and lift-off processes was performed. A 2 nm titanium layer was also evaporated to improve the adhesion of the Au disk to the silicon surface. Finally, a micron-thickness silicon dioxide uppercladding was deposited on the samples by using a Plasma Enhanced Chemical Vapour Deposition (PECVD) system from Applied Materials.

Besides the active region, the output waveguides were made long enough to carry out the polarization-dependent optical power in each mode to the chip boundary, from which they could be detected by using an infrared camera as shown in Fig. S7.

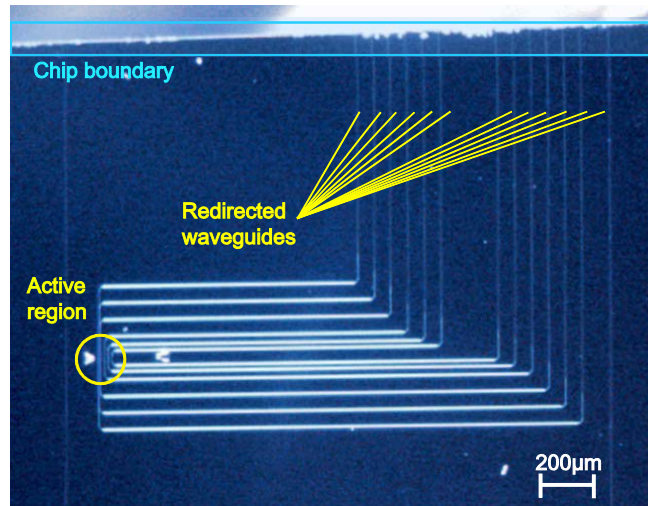


Figure S7. Optical microscope image of a fabricated sample. Note that the optical waveguides coming from the active region are redirected to the chip boundary in order to capture them simultaneously with the infrared camera. The scatterers are placed in the so-called active region, where SOI takes place.

S.5. Experimental measurements

In order to retrieve the input SoP, we consider each nanoantenna port-mode combination k as an independent polarization analyzer. For the case of the waveguide with the single scatterer, if we

make use of the fundamental even and odd modes (TE and TM-like modes) at both output ports, the polarimeter has $Q = 4$ polarization analyzers. Thus, it will be able to retrieve the input SoP as long as the polarimetric matrix \mathbf{W} is invertible, which is achieved by breaking the mirror symmetry so that SOI plays a role, as previously discussed. Each polarization analyzer is characterized by an analyzer vector - defined equivalently to a Stokes vector [6] -containing four elements, as defined in Eq. (2.15). In the analyzer vector definition the m parameter takes six different values, which correspond to the six “calibration measurements” we use to conform experimentally the polarimetric matrix \mathbf{W} for each wavelength, which can be written as:

$$\mathbf{W} = \begin{pmatrix} A_{TE,x+}(0) + A_{TE,x+}(\infty) & A_{TE,x+}(0) - A_{TE,x+}(\infty) & A_{TE,x+}(1) - A_{TE,x+}(-1) & A_{TE,x+}(-i) - A_{TE,x+}(i) \\ A_{TM,x+}(0) + A_{TM,x+}(\infty) & A_{TM,x+}(0) - A_{TM,x+}(\infty) & A_{TM,x+}(1) - A_{TM,x+}(-1) & A_{TM,x+}(-i) - A_{TM,x+}(i) \\ A_{TE,x-}(0) + A_{TE,x-}(\infty) & A_{TE,x-}(0) - A_{TE,x-}(\infty) & A_{TE,x-}(1) - A_{TE,x-}(-1) & A_{TE,x-}(-i) - A_{TE,x-}(i) \\ A_{TM,x-}(0) + A_{TM,x-}(\infty) & A_{TM,x-}(0) - A_{TM,x-}(\infty) & A_{TM,x-}(1) - A_{TM,x-}(-1) & A_{TM,x-}(-i) - A_{TM,x-}(i) \end{pmatrix} \quad (5.1)$$

Where each element $A_{n,x\pm}(m)$ is the effective area of the analyzer provided by the n -th guided mode propagating forwards (+) or backwards (-) when the polarimeter is excited by an incoming polarization defined by m . After calibration, we will be able to reconstruct the incident SoP (\mathbf{S}) by measuring the optical power at the four outputs (\mathbf{P}) for a given wavelength and applying:

$$\mathbf{S} = \mathbf{W}^{-1}\mathbf{P}/I_{\text{inc}} \quad (5.2)$$

We demonstrated experimentally the performance of several fabricated Stokes nanopolarimeters at telecom wavelengths. The measurement set-up is depicted in Fig. 3a of the main text. Here, we describe it in more detail. A tunable laser at wavelengths covering the range between 1320 and 1630 nm was used as light source, controlling the polarization at its output with a fiber polarization controller. The optical power generated by the laser was of the order of 1 mW. The subwavelength active region of the sample (this is, the region containing the scatterer coupled to the waveguide in which SOI takes place) was illuminated from a cleaved optical fiber with a special final section containing a 2 mm long quarter wave plate (QWP) provided by Fibercore in order to allow the circularly and elliptically polarized light illumination. The vertical placement of the sample (see Fig. S7) creates two orthogonal paths. In the horizontal path, the illuminating light propagates through the silicon substrate, so the polarization was monitored by using an objective for collimating the radiation passing through the silicon substrate and a free-space linear polarizer (FPC). Once the light passed through the FPC a 50:50 splitter was used to split up the power between a power meter (Newport 1930C) and an IR camera (Indigo Alpha NIR). Linear input polarizations were obtained by minimizing the orthogonal polarization component reaching an axial ratio $> 20\text{dB}$. We used an extra QWP between the objective and the FPC for monitoring circular and elliptical input polarizations (see Fig. 3A). This allowed us to convert such inputs into linear polarization, which was detected. We checked the achievement of purely circular polarizations by removing the QWP afterwards (axial ratios of the order of 0.5dB were measured). The vertical path was used to recover the optical output power of the polarimeter waveguides with a IR camera (Xenics XS-XC117) mounted at the position of the eyepiece of a $4\times$ microscope (National Stereoscopic Microscopes Zoom model 420 series), focused on the waveguide outputs (Fig. S8a). An FPC placed horizontally between the waveguide outputs and the microscope was required in order to separate the TE and TM-like outputs of the polarimeter. We integrated the camera counts in the scattering spots so as to capture the spot intensity in each output port (Fig. S8b).

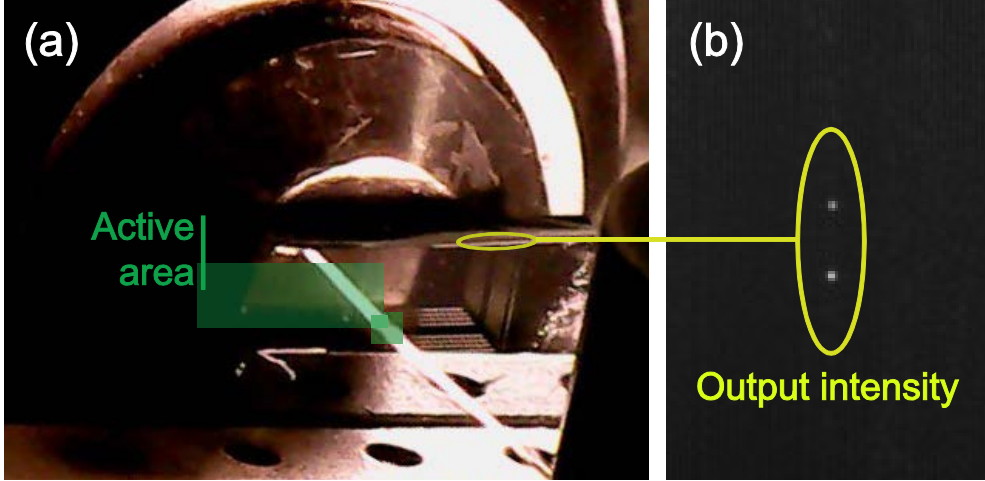


Figure S8. (a) Image of the sample mount in the experimental setup, where the optical fiber is aligned to the active area of the chip. The fabricated system was replicated 3 times and all output ports were redirected vertically. (b) Image of the output port spots captured by the IR camera, coupled to the microscope.

Notice that this experimental set-up is possible because of the non-destructive nature of the polarimetric approach: the light passing through the chip is only slightly depolarized because of the extraction of a tiny amount of power (which will depend on the SoP of the signal) so the polarization can be simultaneously detected in the vertical (via the nanopolarimeter) and the horizontal (via common free-space polarimetric elements) paths. Therefore, as in [9], our approach can operate in-line and would be suitable for fast-tracking of the SoP in nodes of optical networks.

To conform the polarimetric matrix \mathbf{W} we obtained the response of the polarimeter for the six “calibration polarizations” (i.e. vertical, horizontal, 45° and 135° linear polarizations and right, left-handed circular polarizations). We configured the input SoP using the fiber polarization controller while monitoring the polarization with the horizontal path of the experimental setup, and we measured the four output powers of the polarimeter as explained above. Then we formed the \mathbf{W} matrix from these measurements by applying (5.2). The experimental result of the \mathbf{W} matrix, obtained by measuring the spot intensities in camera counts of a fabricated T-block shaped polarimeter for a wavelength of 1558 nm (as the results shown in Fig. 3) is:

$$\mathbf{W} = \begin{pmatrix} 54.69 & -46.24 & -42.55 & 24.34 \\ 127.12 & -78.88 & 71.21 & -75.46 \\ 188.10 & 3.78 & 177.99 & 66.22 \\ 105.32 & 61.08 & -168.92 & -89.92 \end{pmatrix} \quad (5.3)$$

Once the polarimetric matrix was known we impinged in the active area of the nanopolarimeter with a set of different input polarizations, where the angle, ellipticity and handedness were varied. We captured all spot intensities for each input polarization and subtracted the background noise collected by the IR camera in the same region without spot. The experimental results of the four output spot intensities for a set of linear polarization measurements are depicted in Fig. S9. Once the output power was collected, we recovered the SoP by applying Eq. (5.3).

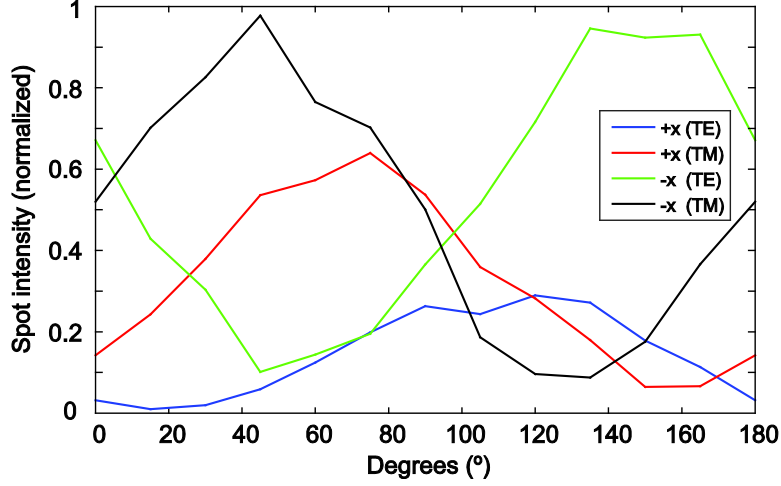


Figure S9. Experimentally measured output spot intensities for a set of different input linear polarizations, normalized respect to the maximum spot intensity. Note that the response of the system has a sine-like variation.

Moreover, we tested these devices at other wavelengths so as to ensure its broad bandwidth even though the performance is not optimal. To change the operational wavelength, we re-calibrated the polarimeter -i.e. form the polarimetric matrix \mathbf{W} . The results for three different wavelengths are shown in Fig. S10, where the Stokes parameters of the input SoP (blue) and the recovered SoP by the polarimeter (red) are depicted. The selected wavelengths for testing the device were 1550 nm, 1520 nm and 1300nm for the rectangular scatterer polarimeter and 1550 nm, 1567 nm and 1619 nm for the T-block shaped polarimeter, in which we can observe that the experimental results match with the expected behavior of the device. These results confirm that our device could be used for spectropolarimetry.

S.6. Response to unpolarized light

So far we have only considered the response of our SOI nanopolarimeter for fully polarized light. However, it makes sense to consider how its response will be in the case of unpolarized light. In the case that monochromatic fully unpolarized light impinges on our SOI polarimeter, we can assume that there will not be SOI-related effects. As so, for each mode, light will be equally scattered in the x+ and x- directions due to the symmetry of the structure, which by definition cannot be broken by unpolarized light. This is exactly what the polarimetric approach predicts when unpolarized light impinges on a polarimeter. The power measurement at the outputs is given by $\mathbf{P} = I_{\text{inc}} \mathbf{W} \mathbf{S}$, which for fully unpolarized light $\mathbf{S} = (1,0,0,0)^T$ corresponds to selecting the first column of the polarimetric matrix \mathbf{W} . The matrix \mathbf{W} is given by the rows in Eq. (2.14). Knowing from Eq. (2.6) that $A_k^{\text{max}} = |l_H^k|^2 + |l_V^k|^2$, we can immediately see that the power measurement predicted for fully unpolarized light is given by the simple expression $\mathbf{P} = (P_{\text{TE}}^{x+}, P_{\text{TE}}^{x-}, P_{\text{TM}}^{x+}, P_{\text{TM}}^{x-})^T = I_{\text{inc}} (0.5 A_{\text{TE}}^{\text{max}}, 0.5 A_{\text{TE}}^{\text{max}}, 0.5 A_{\text{TM}}^{\text{max}}, 0.5 A_{\text{TM}}^{\text{max}})^T$, or more generally for an arbitrary polarimeter (with no need to assume mirror symmetries) we get $P_k = 0.5 A_k^{\text{max}}$. This effective area corresponds to the averaged effective area over the whole Poincare sphere of polarizations $\oint A_k^{\text{eff}} dS / \oint 1 dS = 0.5 A_k^{\text{max}}$ for each port-mode combination (see Figure S3). This power measurement corresponds exactly to what one would expect for fully unpolarized light impinging on our scatterers.

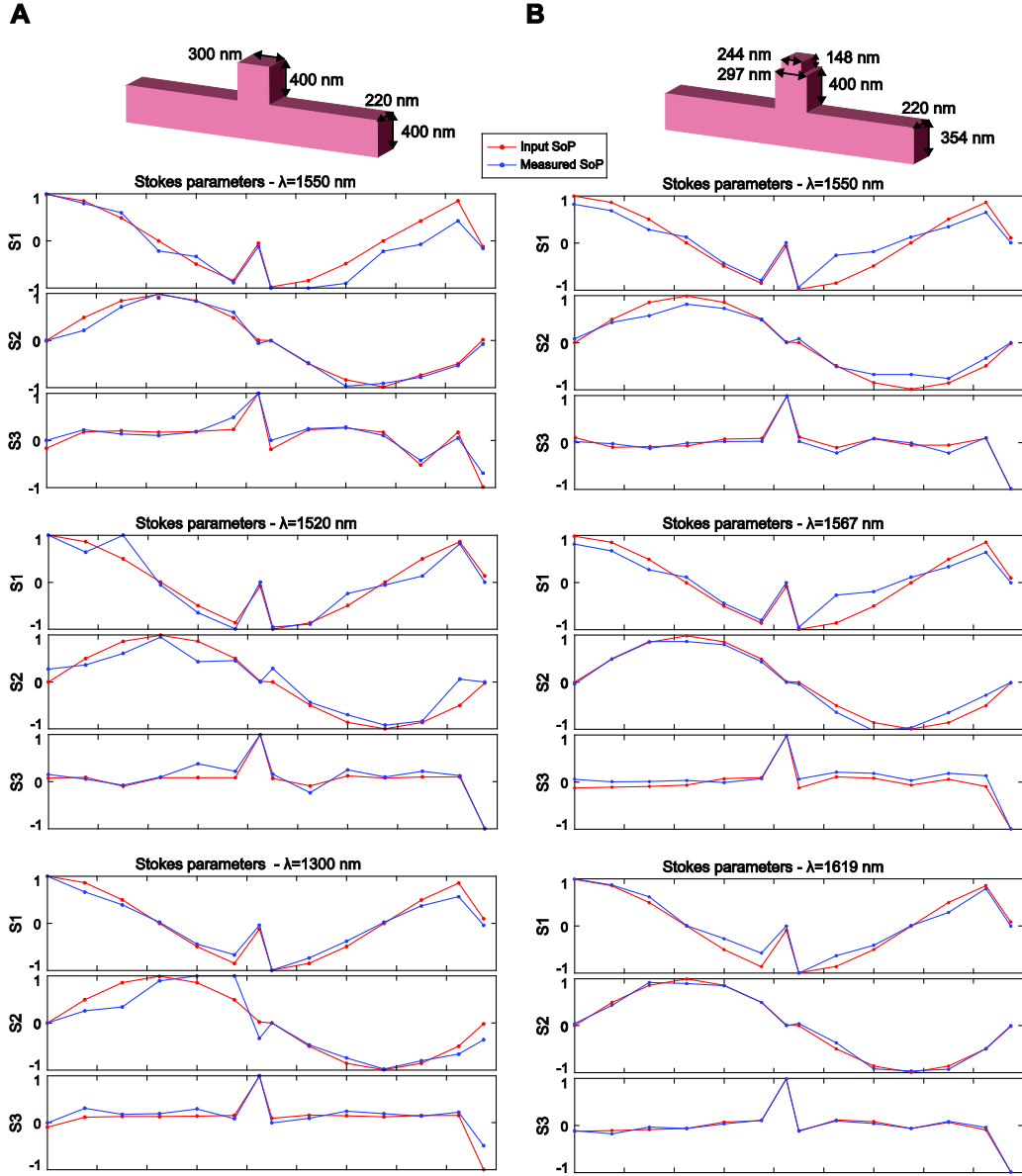


Figure S10. Experimental results of the input and recovered SoP represented using the Stokes parameters S_1 , S_2 and S_3 for different wavelengths and designs. In A is depicted the response of the initial rectangular polarimeter for wavelengths 1550 nm, 1520 nm and 1300 nm, while in B is depicted the optimized T-block shaped polarimeter response for wavelengths 1550 nm, 1567 nm and 1619 nm. A set of input polarization is depicted in red, where the angle, ellipticity and handedness is modified. The recovered polarization by the Stokes nanopolarimeter is depicted in blue.

We also performed a simple check from our measurements. We used the \mathbf{W} matrix retrieved experimentally (Eq. 5.3) and we considered what would happen if we illuminated the polarimeter with a source that switches its polarization randomly between two orthogonal polarizations, spending 50% of the time on each, when the switching rate approaches infinity. This source would constitute a completely unpolarised source. We can select two orthogonal polarizations that we have a measurement for, such as linearly polarized light at 15° and 105° (both different to the calibration polarizations). Each has a power measurement vector which corresponds to the four measurements at each port-waveguide output, and which we determined experimentally to be $\mathbf{P}_{15} = (3.78, 97.21, 280.79, 171.53)$ and $\mathbf{P}_{105} = (97.42, 143.68, 74.51, 205.86)$, in units of camera

counts. If the switching rate between both states is very fast, the camera will detect an average of the two intensity measurements, so it will detect a vector $\mathbf{P} = (\mathbf{P}_{15} + \mathbf{P}_{105})/2 = (50.6, 120.45, 177.65, 188.7)$, which would be the power vector measured for this particular un-polarized source. Applying the experimental \mathbf{W} matrix (Eq. 5.3) to this vector, we retrieve the Stokes vector as $\mathbf{S} = (1.000, 0.000, 0.000, 0.000)$, corresponding to fully unpolarized light, as expected. Notice that contrary to the theoretical considerations above, in this case the two opposite outputs for each mode do not carry equal power. This can be ascribed to fabrication imperfections on the scatterer and to experimental power imbalances such as unequal waveguide losses and out-coupling efficiencies. However, matrix \mathbf{W} is experimentally calibrated, and therefore automatically accounts for these imbalances, giving the correct result for unpolarized light.

Supporting References

- [1] Espinosa-Soria, A.; Martinez, A. *IEEE Photon. Technol. Lett.* **2016**, 28, 1561-1564.
- [2] Bliokh, K. Y.; Smirnova, D.; Nori, F. *Science* **2015**, 348, 1448-1451.
- [3] Aiello, A.; Puentes, G.; Voigt, D.; Woerdman, J. P. *Opt. Lett.* **2006**, 31, 817-819.
- [4] Peinado, A.; Lizana, A.; Vidal, J.; Iemmi, C.; Campos, J. *Opt. Express* **2010**, 18, 9815-9830.
- [5] Bliokh, K. Y.; Bekshaev, A. Y.; Nori, F. *Nat. Commun.* **2014**, 5, 3300.
- [6] Chipman, R. A. "Polarimetry," in *Handbook of Optics*, M. Bass, ed. The McGraw-Hill Companies, Inc., **2010**.
- [7] Tyo, J. S. *Appl. Opt.* 2002, 41, 619-630.
- [8] Foreman, M. R.; Favaro, A.; Aiello, A. *Phys. Rev. Lett.* **2015**, 115, 263901.
- [9] Balthasar Mueller, J. P.; Leosson, K.; Capasso, F. *Optica* **2016**, 3, 42-47.
- [10] Rodríguez-Fortuño, F. J.; Puerto, D.; Griol, A.; Bellieres, L.; Martí, J.; Martínez, A. *Opt. Lett.* **2014**, 39, 1394-1397.
- [11] Rodríguez-Fortuño, F. J.; Puerto, D.; Griol, A.; Bellieres, L.; Martí, J.; Martínez, A. *Laser Photonics Rev.* **2014**, 8, L27-L31.